Structural and functional highlights of methionine aminopeptidase 2 from Leishmania donovani

Saleem Yousuf Bhat, Arijit Dey, Insaf A. Qureshi

PII: S0141-8130(18)30321-0
DOI: doi:10.1016/j.ijbiomac.2018.04.090
Reference: BIOMAC 9498

To appear in:

Received date: 18 January 2018
Revised date: 16 April 2018
Accepted date: 17 April 2018

Please cite this article as: Saleem Yousuf Bhat, Arijit Dey, Insaf A. Qureshi , Structural and functional highlights of methionine aminopeptidase 2 from Leishmania donovani. The address for the corresponding author was captured as affiliation for all authors. Please check if appropriate. Biomac(2017), doi:10.1016/j.ijbiomac.2018.04.090

Structural and Functional Highlights of Methionine Aminopeptidase 2 from *Leishmania donovani*

Saleem Yousuf Bhat, Arijit Dey and Insaf A. Qureshi*

Department of Biotechnology & Bioinformatics, School of Life Sciences, University of Hyderabad, Prof. C.R. Rao Road, Hyderabad 500046, India

*Correspondence E-mail: insaf@uohyd.ac.in

Abstract

Methionine aminopeptidase 2 (MAP2) is a principal regulator of apoptosis for *Leishmania donovani* and a potential candidate for the design and synthesis of novel antileishmanials. The *Ld*MAP2 gene was cloned in pET28a(+)-SUMO vector, expressed in *E. coli* and then purified by chromatographic methods. It was found to be a monomer and required divalent metal ion for its activity against synthetic substrates with Co(II), Mg(II), Mn(II) and Ni(II) being the major activators. Moreover, Ca(II) showed the tightest binding with K_m value of 124.7±9.2 μM, while Co(II) proved most efficient for catalysis with k_{cat} value of 128.1±4 min^{-1}. The naturally occurring aminopeptidase B inhibitor bestatin was found to be a potent inhibitor of *Ld*MAP2 with a K_i value of 0.86 μM. Further, structural studies with circular dichroism (CD) showed an increase in the α-helical and β-sheet contents and a decrease in random coils in *Ld*MAP2 upon interactions with both bestatin and fluorogenic substrates. Finally, structural studies pointed out key differences in the structure of *Ld*MAP2 and *Hs*MAP2 and their interactions with inhibitor bestatin, Ala-AMC, Leu-AMC and Met-AMC. The structural differences of two orthologs and different binding modes with bestatin can be crucial for the development of novel and specific inhibitor against leishmaniasis.

Keywords

Methionine aminopeptidase 2; *Leishmania donovani*; enzyme kinetics; bestatin; molecular docking; molecular dynamics studies

Introduction

Protozoan dimorphic parasites of genus *Leishmania* cause leishmaniasis which is characterized by a wide spectrum of clinical manifestations that includes ulcerative skin lesions to life-threatening visceral infections. *Leishmania* parasites are transmitted through the bite of sandfly to the mammalian hosts [1]. Approximately 12 million people are affected by leishmaniasis in 80 countries with about 4,00,000 new cases reported each year [2]. There are estimates of about 70,000 deaths occurring annually and a further 350 million at risk of getting infected [3]. Due to the unavailability of any significant vaccination, chemotherapy along with vector control, continue to remain a significant element in the control of all forms of leishmaniasis. The prominent antileishmanials used currently include pentavalent antimony, amphotericin B and miltefosine. Even though effective, the current line of antileishmanials are toxic, unaffordable and carry a risk of turning ineffective due to the emergence of drug resistant parasites [4][5]. This highlights the need to design and develop new drugs against leishmaniasis. Aminopeptidases are exopeptidases catalyzing the cleavage of amino acids from N-terminal in proteins and peptides [6]. The metal dependent aminopeptidase-catalyzed degradation of smaller peptides in the terminal stages of protein degradation pathway provides free amino acids to the organism [7][8]. The genome of *L. donovani* encodes at least twelve aminopeptidases most of which belong to the M1, M20, M18, M17 and M24 aminopeptidases. There are several reports of these proteins to be druggable targets against many adversaries like cancer and malaria [9][10].

Methionine aminopeptidases (MAPs) are ubiquitous and highly conserved metal dependent hydrolases that remove N-terminal initiator methionine from nascent polypeptides either co-translationally or post-translationally [11] and belong to the M24 class of peptidases as per the MEROPS peptidase database classification (https://merops.sanger.ac.uk/). The excision of initiator methionine amino acid residue is a prerequisite for further posttranslational

modifications of nascent polypeptides *viz.* myristoylation, localization, proper folding, and protein activity in both prokaryotes and eukaryotes [12][13][14]. To hydrolyze the methionyl amino acid residue in the ultimate position, MAPs require a small uncharged residue (usually Gly or Ala) at the penultimate position of the nascent polypeptide chain [15].

MAPs are grouped into two categories: type I (MAP 1) and type II (MAP 2), with the unique insertion of nearly 60 amino acids residues in MAP2 at the C terminus of the catalytic domain [16]. While as, the MAPs of prokaryotic bacteria and archaea contain the minimal catalytic domain, MAPs of eukaryotes possess additional *N*-terminal domains [17] *viz.* the occurrence of *N*-terminal zinc-finger motif (like in human or yeast MAPs) or the existence of a polybasic/polyacidic domain like the one reported for human MAP type IIb that is responsible for the phosphorylation blockade of eukaryotic initiation factor 2a subunit [18]. Notably, eukaryotes harbour both isoforms unlike prokaryotic genomes that encode only one isoform: type I in bacteria and type II in archaea [19]. A previous report on the abundance of two isoforms in eukaryotes suggests MAP1 to be constitutively expressed and is thence considered as a house-keeping enzyme. On the contrary, MAP2 expression is regulated by extra-cellular signals and cell cycle status [20].

MAPs require divalent transition metal ions as cofactors for activity [21]. Previous studies on MAPs from different organisms indicate cobalt ions to be the most preferred divalent metal activator [22]. However, MAPs also exhibit activity with other divalent cations like Mn(II), Ca(II), Ni(II) or Fe(II) [23]. In contrast, Zn(II) is not a very suitable metal cofactor for the amidolytic activity of most MAPs [24]. The lethal phenotypes developed by MAP knockouts in both prokaryotes and eukaryotes highlights the importance of this family of enzymes [25][26]. A recent report on *Ld*MAP2 suggests it to be a key regulator of apoptosis for the human parasite *L. donovani* [27]. Moreover, given their essentiality [25], MAPs are emerging as potential targets for the discovery of novel chemotherapeutics to combat bacterial,

microsporidial and parasitical organisms [28][29][13]. The specific inhibitors of MAP2 like fumagillin and its derivatives have captivated interest in medicine as pro-drugs for diseases like obesity and cancer [30][31][32][33]. Even though in clinical trials as a potent inhibitor of MAP2, the use of pro-drug TNP-470 hasn't captivated interest in the recent years due to reports of its toxicity [34][35]. This highlights the need to find newer drugs which are small, potent, highly specific and affordable.

We herein report our findings on the expression, purification, and characterization of *Ld*MAP2 as well as its interaction and inhibition with aminopeptidase inhibitor bestatin. We also show recombinant *Ld*MAP2 to be active in the MAP2 enzymatic assay against fluorogenic substrates. The structural analysis using *in silico* approach suggests key differences between the human and parasitic orthologs in the MAP2 prosite, catalytic pocket and a different binding mode to broad-spectrum aminopeptidase inhibitor bestatin pointing towards its suitability as a new druggable target. Our results also suggest *Ld*MAP2 to have more affinity towards divalent calcium paving way for its use as a non-toxic biocatalyst.

Materials and methods

Bacterial strains, plasmids, and enzymes

The competent *E. coli* DH5-alpha and BL21 (DE3) cells utilised for cloning procedures and protein expression respectively were procured from Invitrogen (USA). The expression plasmid pET28a-SUMO was generously gifted by Dr Mohd Akif of the Department of Biochemistry, University of Hyderabad. *Taq* polymerase, Phusion polymerase, restriction enzymes and T4 ligase were procured from Thermo Scientific (USA).

Sequence analysis and cloning of *Ld*MAP2

The *Ld*MAP2 sequence comprising of 465 amino acid residues was retrieved from the online database KEGG (http://www.genome.jp/kegg/). The protein sequence was subjected to Pfam [36], TOPCONS [37] and Expasy Protparam [38] tool for sequence analysis. The full length *Ld*MAP2 ORF (1398 nucleotides) was amplified by PCR at an annealing temperature of 58°C from the genomic DNA of *Leishmania donovani* using gene specific primers as, forward primer 5' TATGGATCCCCACCAAAGATGTCTGCGAAAAAC 3' and reverse primer 5' CATCTCGAGCTAGTAGTCGCTTCCCTTGGAAAG 3'. The amplicon was extracted and purified with GeneJet DNA extraction kit (Thermo Scientific, USA) and digested overnight at 37°C with restriction enzymes *Bam*HI and *Xho*I (Thermo Scientific, USA). The *Ld*MAP2 insert was then purified again and put in frame between the restriction sites of *Bam*HI and *Xho*I of the plasmid expression vector pET28a(+)-SUMO. The clone was confirmed with DNA sequencing (CDFD, Hyderabad) to corroborate the *Ld*MAP2 sequence.

Expression and purification of *Ld*MAP2

The *E. coli* BL21 (DE3) competent cells for protein expression were transformed with *Ld*MAP2 clone using a standard transformation procedure. The expression cells transformed with *Ld*MAP2 were cultured overnight in Luria-Bertani (LB) media carrying 50 μg/ml kanamycin at 37°C in a shaking incubator. Afterwards, the LB media with 50 μg/ml kanamycin were inoculated by 1 percent of the starter culture and the culture grown at 37°C till an OD of 0.5 was obtained at 600 nm. Subsequently, the expression of *Ld*MAP2 was induced by 0.5 mM isopropyl-1-thio-β-D-galactopyranoside (IPTG). The culture was then further grown at 37°C for 4 hours before being harvested by centrifugation at 5000 rpm for 20-25 min at 4°C. For protein purification procedures, the cells were suspended in lysis buffer (50 mM Tris-HCl pH 8.0, 400 mM NaCl, 5% glycerol, 25 mM imidazole) followed by cell lysis using sonication at a pulse break ratio of 10:10 with 35% amplitude. A DNase

treatment in the presence of 10 μm $MgCl_2$ was given to the cell lysate before centrifugation at 14,000 rpm for 45 minutes at 4°C to remove the cell debris. Finally, the soluble recombinant *Ld*MAP2 protein in the supernatant was allowed to bind to a pre-packed His-trap purification column (GE Healthcare) with a constant flow rate of 0.5 ml/min on AKTA purification system (GE Healthcare). After rigorous washing to ward off the non-specificities, the protein was eluted by elution buffer which was comprised of 50 mM Tris-HCl pH 8.0, 400 mM NaCl, 5% glycerol and 250 mM imidazole.

To remove metal contaminants, EDTA was incorporated to the pure protein to a final concentration of 1mM which was later removed by extensive dialysis. To excise the N-terminal SUMO-tag, SUMO protease (purified separately by affinity chromatography) was added to the pure protein in 1:100 ratio and subjected to dialysis for 12-16 hours at 4°C in 50 mM Tris-HCl pH 8.0 and 100 mM NaCl. The digested protein was again passed through His-trap purification column to cause the entrapment of SUMO tag and SUMO protease as both carry an N-terminal 6X His-tag. While as, the pure protein was collected in the flow through and then protein quality analysed with 10% (w/v) SDS-PAGE.

Consequently, *Ld*MAP2 was concentrated with a 10 kDa Millipore concentrator and the volume reduced to 1 ml or less. For buffer exchange, size-exclusion chromatography using Superdex™75 10/300 GL column (GE Healthcare) was performed with a buffer containing 50 mM Tris-HCl pH 8.0, 150 mM NaCl. The purity of the recombinant *Ld*MAP2 was verified by SDS-PAGE and the protein concentration was determined on Nano drop (Thermo Scientific, USA) using molar absorption coefficient of 46870 mol^{-1} cm^{-1} and molecular weight of 51300 Da (computed using ExPASy- ProtParam).

Enzyme activity assay

The aminopeptidase activity of *Ld*MAP2 was assessed by recording the rate of liberation of L-methionine, L-leucine and L-alanine from three fluorogenic substrates i.e. methionine-4-

methyl-coumaryl-7-amide, leucine-4-methyl-coumaryl-7-amide, and alanine-4-methyl-coumaryl-7-amide (Sigma Aldrich, USA). The released florescent product (AMC) was measured using Infinite M200 Pro spectrofluorometer (TECAN, Switzerland) with specific wavelength pairs suggested by the manufacturer for emission and excitation and as reported previously [39][40] with modifications wherever necessary. To determine the pH optima for aminopeptidase activity, 50 mM acetate buffer (pH 3.5, 4.5 and 5.5), 50 mM MES (pH 6.5), 50 mM Tris–HCl, pH (7.5–8.5) and 100 mM CAPS (pH 9.5) were used. All buffers used were supplemented with 100 μM $CoCl_2$ and 0.1 μM *Ld*MAP2 for activity. After activation at 37°C for 30 minutes, fluorogenic substrate (0.2 mM) was added and the activity was measured at 37°C. The divalent metal ion requirement was investigated by assaying the *Ld*MAP2 activity after pre-incubating the enzyme at 37°C for 30 minutes in 50 mM Tris–HCl (pH 8.0) containing a different metal chloride independently (HiMedia Laboratories, India).

Enzyme kinetics

The steady state kinetic parameters K_m and V_{max} of *Ld*MAP2 were determined by pre-incubating the enzyme with 100 μM of metal chloride for 30 minutes at 37°C as reported previously [40] with necessary modifications. The amidolytic activity was measured in the substrate concentration range of 10-400 μM with each well blanked by the respective substrate blank while data plotting. The linear portions of the florescence versus time curve were used to determine the initial velocity and the k_{cat} determined by converting the florescence to AMC using an AMC standard curve. The K_m and V_{max} values were determined from three independent experiments performed under same conditions.

Influence of metal cofactors

To determine the best divalent activator of *Ld*MAP2, the apo-enzyme was pre-incubated at 37°C for 30 minutes in reaction buffer supplemented with metal chlorides of Co(II), Mg(II), Mn(II), Ca(II), Cu(II), Ni(II), Fe(II) and Zn(II) in final assay concentrations of 0.1, 10, 100,

250, 500, 1000, 5000 and 10000 μM in Tris-HCl buffer (50 mM) at a pH optimum of 7.5. For every measurement, a control with no metal cofactor was used to reflect the metal dependence of *Ld*MAP2.

Stability, substrate specificity and inhibition with bestatin

*Ld*MAP2 temperature stability was assessed at seven different pre-incubation temperatures with the standard condition for activity assays being between 35 and 40°C. The apo-enzyme was prepared in reaction buffer supplemented with 100 μM $CoCl_2$ as a cofactor. The reaction mixtures were pre-incubated separately at 10. 20, 30, 40, 50, 60 and 70°C and the reaction started by adding 200 μM of substrate. After incubation at specified temperatures for 30 minutes, the released AMC was recorded using Infinite M200 Pro spectrofluorometer (TECAN, Switzerland). To study substrate specificity, three different fluorogenic substrates (Ala-AMC, Leu-AMC, Met-AMC) were used and the activity of *Ld*MAP2 for each substrate recorded in triplicates. Furthermore, to evaluate the inhibitory efficacy of bestatin, the protein was pre-incubated with 100 μM $CoCl_2$ and varying concentrations of bestatin (1-50 μM) for 30 minutes at 37°C. This was followed by the addition of substrate and the measurement of residual activity at 37°C for 60 minutes with a break of 3 minutes between measurements.

Circular Dichroism (CD) Spectroscopy

CD spectra of *Ld*MAP2 in the presence of substrates and substrate analog bestatin were recorded on JASCO-J1500 CD spectropolarimeter in a quartz cell with a path length of 0.2 cm. The spectropolarimeter was set to accumulate three scans for each spectra at a scan speed of 50 nm min^{-1}. The data was collected at every nanometer from 190 to 250 nm with the final concentration of *Ld*MAP2 used at 0.003 mM. The concentrations of substrates and substrate analog were in the range of 0.001-0.010 mM. To study thermo-stability of *Ld*MAP2, spectral changes were recorded in the temperature range of 20 to 100°C. The Gibbs free energy of unfolding (ΔG) was determined by denaturing the protein with urea (10 mM- 6 M). Besides,

three scans were accumulated in the far-UV region for protein in the pH range of 3.5 to 9.5. The secondary structure content of *Ld*MAP2 and the changes underwent by it were analyzed using the K2D algorithm available on DICHROWEB [41].

Homology modelling and Molecular docking

The program Modeller 9.15 version [42] was used to predict the three-dimensional structure of *Ld*MAP2 by satisfying its spatial restraints using a template with high identity, coverage and similarity to the query *Ld*MAP2sequence. The program BLAST-P was used to search similar crystallographic protein structures with crystal structure of human MAP2 (PDB ID: 1BN5) chosen as template for homology modelling. After fixing the Ramachandran outliers and loop refinement with ModLoop [43], energy minimization was performed with Gromacs 4.6.3 [44]. The geometry of the model was analysed with RAMPAGE [45] and the *Ld*MAP2 structure visualized using PyMOL [46]. The energy minimized structure of *Ld*MAP2 was used for molecular docking using AutoDockVina1.1.2 version [47]. The structural coordinates of substrates i.e. leucine-4-methyl-coumaryl-7-amide, methionine-4-methyl-coumaryl-7-amide, alanine-4-methyl-coumaryl-7-amide and the inhibitor bestatin were retrieved from the online database Pubchem [48], and the geometry was optimized with Discovery studio 3.5 software [49]. To define all possible binding sites and to have structural inputs, a grid based procedure was followed [50]. The macromolecule and ligands were saved as PDBQT files as input files for Autodock Vina. The grid dimension used was 80x88x80 points for blind docking on the macromolecule by the program AutoGrid with a spacing of 0.608 Å. All other parameters were inserted at their default settings.

Molecular Dynamics Simulations

Molecular dynamics simulations were executed with Gromacs 4.6.3 [44] using GROMACS 96 as a force field and SPC as water model for 30 ns for both native *Ld*MAP2 and *Ld*MAP2-bestatin complex as reported previously [51] with certain modifications. For *Ld*MAP2-

bestatin complex, the docking conformation with highest binding affinity was selected. The topology and itp files for bestatin were generated from PRODRG server [52] and added to *Ld*MAP2 topology file to generate a complex topology file. Then, the simulations of native protein and *Ld*MAP2 with bestatin were done in water as solvent with SPC model in a cubic box. To neutralize the system, eight Na^+ ions were added by replacing the solvent (H_2O) molecules. Energy minimization was executed by the steepest decent method for 5000 steps. The application of retardants to the ligand and temperature coupling group treatments were imparted during all simulations. Using GROMACS genester module, the itp file for the bestatin was generated and this information was included in the topology file. A special index group of protein and bestatin was created using make_ndx module to treat protein and ligand separately followed by equilibration Phase I (NVT) and Phase II (NPT) for 50 ps before setting up a run for 30 ns production simulations at 300K. All MD simulations and results analysis were performed with the 16 node OSCAR Linux cluster at the Bioinformatics Facility of School of Life Sciences, University of Hyderabad, India.

Results and discussion

Protein sequence analysis of *Ld*MAP2

The Expasy Protparam tool revealed the protein to be 465 residues long with an approximate molecular weight of 51.30 kDa. The theoretical pI value and the instability index of the sequence were computed to be 6.64 and 44.50 respectively. Besides, the aliphatic index was found to be 69.68 and the grand total average of hydropathicity being -0.620 making the protein slightly hydrophobic. The analysis with TOPCONS revealed no trans-membrane region or signal peptide sequence in the *Ld*MAP2 sequence. While as, the Pfam program displayed a two domain organisation of *Ld*MAP2 like other members of M24 aminopeptidases [53]. The cloned sequence carries a MAP2 signature motif

DVCKLDFGVHVNGYIID which matches the general prosite motif of this class of aminopeptidases DA-LIVMY-x-K-LIVM-D-x-G-x-HQ-LIVM-DNS-G-x(3)-D [54]. The sequence alignment of *Ld*MAP2 sequence with human MAP2 revealed the catalytic residues to be conserved in two orthologs. Consequent to the multiple amino acid substitutions in signature motif of *Ld*MAP2 and the presence of different residues near the prosite, the structure assumed different conformation and a slightly different active site organization which may prove significant for drug design. The multiple sequence alignment reflects nearly 57% sequence identity of *Ld*MAP2 with human MAP2 (Fig. 1). Previous reports suggest MAP2 enzymes to be cobalt activated proteins with two cobalt ions bound to two aspartic acids, a histidine and two glutamic acids (D, D, H, E and E) at the active site [16][53].

Cloning, expression and purification of *Ld*MAP2

The full length MAP2 of human parasite *L. donovani* was cloned into the expression vector pET28a(+)-SUMO. DNA sequencing result and sequence alignment of MAP2 sequence with human MAP2 sequence confirmed that the *Ld*MAP2 clone belongs to MAP2 category of M24 methionine aminopeptidases. The protein was expressed in *E. coli* BL21 (DE3) cells and purified by metal affinity chromatography. The quality of protein was checked on 8% (w/v) SDS-PAGE before and after the cleavage of SUMO tag (Fig. 2A). Furthermore, analysis of partition coefficient (k_{av}) versus $\log_{10}$ molecular weight of standard set of proteins with the k_{av} value of recombinant *Ld*MAP2 suggested it to be a monomer (Fig. 2B). Notably, other members of the M24 methionine aminopeptidases (MAPs) including the human MAP2 exist as monomers as well [55][53].

Co(II) is the major activator of *Ld*MAP2 for amidolytic activity against synthetic substrates

The amidolytic activity of *Ld*MAP2was assessed with eight metal chlorides Ca(II), Co(II), Cu(II), Mg(II), Mn(II), Ni(II), Zn(II), and Fe(II) at an optimum metal ion concentration of

100 μM (Fig. 3A, 3B & 3C) and the kinetic parameters determined using Graphpad prism 4.0 (Table 1). The optimal pH for the catalytic activity of *Ld*MAP2 against the fluorogenic substrates used in this study was 7.5 (Fig. 4C and 4D). To ascertain reasons behind less or no activity of *Ld*MAP2 at low and high pH, CD spectra were taken at different pH. The spectra taken at extreme pH recorded a sharp dip in *Ld*MAP2 secondary structural elements particularly at pH 3.5 and pH 9.5 where protein had lost significant secondary structure. The protein had highest secondary structural content at pH 7.5 and thence more catalytic activity (Fig. 4D) much like other MAPs [24][19]. Although *Ld*MAP2 exhibited highest enzyme activity with Co(II), the Km was least when *Ld*MAP2 was activated by Ca(II). This suggests the high affinity of Ca(II) for *Ld*MAP2 (Table 1), while Zn(II) activated *Ld*MAP2 like its human counterpart showed negligible amidolytic activity towards the fluorogenic substrates [22]. The Co(II) or Ca(II) activated *Ld*MAP2 was largely active at all metal concentrations below1000 μM. However, activity diminished significantly at higher concentrations possibly due to the interference of high metal concentrations in catalysis [16]. Interestingly, the spectra of *Ld*MAP2 taken at higher metal concentration showed significant loss of secondary structure (Fig. 4A and 4B). Additionally, CD results indicated that high concentrations of metal decreased the thermal stability of *Ld*MAP2 as the protein was denatured at apparently lesser temperatures compared to the apoenzyme (Fig. 4F and 4H). The higher activity exhibited by *Ld*MAP2 with Co(II) can be attributed to the formation of low spin trigonal bipyramidal complexes which tend to be more stable than the complexes formed by zinc [56]. Furthermore, the binding of additional solvents leads to high coordination number of cobalt complexes which intensifies the positive charge of divalent cobalt ions and in turn enhances substrate binding and intermediate stabilization [57][58]. Moreover, Mn(II) and Mg(II) activated *Ld*MAP2 resulted in significant activity like *Tb*MAP1 [24], whereas Ni(II), Cu(II) and Fe(II) activated *Ld*MAP2 had a less catalytic efficiency. For Fe(III) or Fe(II) activated

*Ld*MAP2, a feeble activity was noticed at all metal ion concentrations supplemented in the assay buffer.

Influence of temperature and SUMO-tag on *Ld*MAP2 activity

In order to check the effect of temperature on the *Ld*MAP2 activity, a temperature range of 10-90°C with an interval of 10°C was used and the *Ld*MAP2 activity recorded after the addition of substrate Ala-AMC. The *Ld*MAP2 enzyme was stable and exhibited significant aminopeptidase activity up to 50°C (Fig. 4E). Beyond this the aminopeptidase activity declined since the *Ld*MAP2 denatures profusely after 50°C (Fig. 4F). A similar stability pattern was seen for the calcium activated enzyme (Fig. 4H). Furthermore, the enzymatic activities of recombinant *Ld*MAP2 were studied only after the complete cleavage of N-terminal SUMO-tag. The enzymatic activity of *Ld*MAP2 with SUMO tag was lesser when compared to the protein without tag possibly due to the structural alterations or interference caused by this N-terminal tag. Furthermore, in the absence of metal ion or in the presence of a metal chelator (EDTA) in the reaction buffer, the *Ld*MAP2 activity was undetectable. However, the activity of *Ld*MAP2 enhanced steeply in presence of Co(II), Mn(II) or Mg(II) as is the case with other aminopeptidases [22][28].

***Ld*MAP2 prefers smaller synthetic substrate Ala-AMC to Met-AMC or Leu-AMC**

The enzymatic activity of *Ld*MAP2 was determined against three fluorogenic substrates namely leucine-4-methyl-coumaryl-7-amide, methionine-4-methyl-coumaryl-7-amide and alanine-4-methyl-coumaryl-7-amide. The fluorogenic substrate Ala-AMC was used for enzyme activity as aminopeptidase activity of *Ld*MAP2 was found to be poor against the synthetic fluorogenic substrates Met-AMC like its human counterpart [22]. This could be because Met-AMC is a synthetic substrate and doesn't match the physiological substrates of *Ld*MAP2 where it prefers a smaller residue such as Gly or Ala at the pen-ultimate position for cleavage of N-terminal methionine [15]. However, *Ld*MAP2 cleaved smaller amino acid

residue Ala efficiently from the substrate Ala-AMC in comparison to Met-AMC and Leu-AMC which it cleaved poorly and slowly (Fig. 4G). Amongst three substrates, the activity of *Ld*MAP2 was maximum against Ala-AMC suggesting it to be more active in hydrolyzing smaller amino acid residues from synthetic substrates. The activity against Ala-AMC was defined as 100% while comparison of *Ld*MAP2 activity against other fluorogenic substrates.

Bestatin inhibits *Ld*MAP2 in a dose dependent manner

Bestatin is a naturally occurring dipeptide and a prominent metalloaminopeptidase inhibitor produced by *Streptomyces olivoretuculii* (Actinomycetes) [59]. It is reported to inhibit many aminopeptidases including the members of M17 aminopeptidases [60], aminopeptidase B and induces programmed cell death [61]. Besides, bestatin has found use in the treatment of acute myelocytic leukemia [62] and melanoma [63]. Bestatin inhibits other families of aminopeptidases like the M1 and M17 aminopeptidases and has shown potential as a prodrug due to its low toxicity in experimental animals [64][65]. Notably, bestatin has been formulated to use as a drug against squamous cell carcinoma in humans [61]. The major molecular targets of bestatin are the metal dependent aminopeptidases in cells [66]. Bestatin inhibited the enzyme activity of *Ld*MAP2 in *in vitro* inhibition assays in a dose dependent manner (Fig. 5A). Moreover, bestatin proved to be a potent inhibitor of *Ld*MAP2 with a K_i value of 0.86 μM. Analysis of bestatin binding mode with *Ld*MAP2 revealed it to be a competitive inhibitor of *Ld*MAP2 as the binding occurred at the active site like other aminopeptidases inhibited by it [67][68]. The binding mechanism was elucidated by plotting the Line-weaver Burk plot (Fig. 5B) of the uninhibited and inhibited *Ld*MAP2 and docking of bestatin with the modelled structure of *Ld*MAP2 (Fig. 8B). The inhibitory efficacy of bestatin suggests it to be a useful scaffold which can guide the design of novel and small molecule inhibitors for the selective inhibition of *Ld*MAP2.

Addition of bestatin and fluorogenic substrates increased secondary structural elements of *Ld*MAP2

CD spectroscopy was employed to study the changes occurred in *Ld*MAP2 secondary structure upon binding to fluorogenic substrates and bestatin and to study the thermodynamic stability. To calculate Gibbs free energy (ΔG), the spectral data taken at different concentrations of urea was normalized and fitted into two-state unfolding transition [69]. The free energy (ΔG) was computed to be approximately 2.2 kcal mol^{-1} (Fig. 6A and 6B). A concentration dependent increase in the ellipticity at 208 and 222 nm were observed in the CD spectra of *Ld*MAP2 upon addition of its substrates and bestatin. We reasoned that the secondary structural change may have come into existence due to the helix stabilization upon the addition of Ala-AMC, Met-AMC, Leu-AMC and bestatin. This behaviour is already known for a metal dependent aminopeptidase [70] and human serum albumin [71]. The secondary structural elements of *Ld*MAP2 and the changes in the structure thereof were analyzed by using the K2D algorithm of the software program DICHROWEB. In the apo*Ld*MAP2, the secondary structure consists of 28% α-helix, 42% β-sheets and 30% random coils which are in close agreement with the secondary structural elements seen in the 3D structure of *Ld*MAP2. Furthermore, the signal at 208 nm increased predominantly at all concentration of Ala-AMC, Met-AMC, Leu-AMC and bestatin. At 0.010 mM concentration of bestatin, the α-helical content soared to 32%, while the proportion of β-sheets increased to 50% and random coils plunged to 18%, respectively (Fig. 6C and 6D). A similar pattern was observed with synthetic substrates of *Ld*MAP2 used in this study. These results indicate that the secondary structure of *Ld*MAP2 gained more order and random coil declined due to the addition of substrates and bestatin which presumably leads to respective complex formations. The differential changes in *Ld*MAP2 conformation upon binding of bestatin, Ala-AMC, Met-AMC and Leu-AMC may be attributed to differences in the sizes of the amino acid chains of

these substrates. Moreover, it is clearly observed that bestatin has less influence than Ala-AMC, Leu-AMC and Met-AMC which might be due to the larger size of these substrates. The change in the average secondary structure of *Ld*MAP2 may not be due to the flexibility of two domains in the proteins as MDS studies didn't suggest any considerable flexibility in the overall protein structure.

Homology modelling of *Ld*MAP2and molecular docking studies

The full length protein sequence comprised of nearly 100 residues in disordered region at the N-terminus for which multiple searches with BLAST-P didn't find a template. Therefore, *Ld*MAP2 sequence was modelled without the initial 99 amino acid residues. Analysis of the modelled structure with RAMPAGE suggested two residues (S39 and K42) to be in the disallowed regions of the Ramachandran plot. However, when the outliers in the modelled structure were fixed with program ModLoop and the structure subjected to energy minimization with Gromacs 4.6.3, one amino acid residue (proline at seventh position) from the N-terminus was found to be in the disallowed region. We further proceeded for the docking with bestatin and fluorogenic substrates as the residue was far off from the C-terminus catalytic domain and hadn't any effect on the ligand binding of *Ld*MAP2 and the interactions thereof. The superimposition of the modelled and energy minimized structure revealed an RMSD of 0.16Å which suggests trivial differences and great structural conservation between the two structures. The superimposition of the *Ld*MAP2 structure with *Hs*MAP2 structure showed an RMSD of 0.22Å suggesting significant structural similarity between the two orthologs. The modelled *Ld*MAP2 structure is composed of thirteen β-sheets and eight α-helices with four active site residues (D139, H119, E252 and E347) embedded in the β-sheets 3, 7, 9 and 12 respectively. Another catalytic residue D150 is located in the central loop connecting two small β-sheets. Like *Hs*MAP2 [53], *Ld*MAP2 has its active site

located approximately at the centre of central β sheet on the concave face with two adjacent pairs of α helices and a short COOH-terminal tail covering the sheet's convex face (Fig. 7A). Consequently, Autodock Vina 1.1.2 program was employed to understand the interactions of bestatin and other substrates with *Ld*MAP2. Amongst all generated binding conformations between *Ld*MAP2 and ligands, the conformer with the lowest binding free energy in every case was used for further analysis. The docking results showed that all the docked ligands bind at the active site of *Ld*MAP2. However, bestatin and substrate Ala-AMC because of lesser size embedded deep and had strong contacts with *Ld*MAP2 active site when compared with the Met-AMC and Leu-AMC. Interestingly, the latter were not the most favourable substrates for *Ld*MAP2 in the enzymatic assays too. The key substitutions in the MAP2 prosite (Fig. 7B) like the presence of residues V, M and N in *Ld*MAP2 structure confer different interactions to the structure with inhibitor bestatin and substrates Ala-AMC, Met-AMC and Leu-AMC. Bestatin, which proved to be a potent inhibitor of *Ld*MAP2, binds strongly to residues S217, H227, S231 and the active site residue E252 in the catalytic pocket (Fig. 8B). While as, bestatin interacted with only E255 feebly (bond distance 3.49Å) at the catalytic pocket of the crystal structure of *Hs*MAP2 (Fig. 8A). Therefore, the docking studies suggest Met-AMC and Leu-AMC to be less preferred substrates of *Ld*MAP2. This is presumably because of the failure of Met-AMC and Leu-AMC to make a good contact with the active site of *Ld*MAP2 like Ala-AMC and bestatin. After a thorough analysis of the molecular docking studies, it was concluded that the interactions between *Ld*MAP2 and substrates are majorly due to the hydrophobic forces and hydrogen bonding (Fig. 8C-E) which is similar to the atomic interactions reflected in the crystal structures of *Tb*LAP with bestatin [72] and *Pf*M1AAP with bestatin [73].

Bestatin formed a stable complex with *Ld*MAP2 during molecular dynamics studies

The molecular dynamics simulations were used to calculate the stability of the *Ld*MAP2 and its complexes with bestatin. The parameters RMSD and RMSF along with the radius of gyration (Rg) of the protein (*Ld*MAP2) and its complexes were used for the analysis of the rigidity, protein micro-environment and complex stability during 30 ns MD simulations. The system proved to be stable which reflects the authenticity of molecular docking results where bestatin is bound to *Ld*MAP2 at the active site. The root mean square deviation (RMSD) values of atoms in native *Ld*MAP2 and *Ld*MAP2-bestatin complex were plotted from 0 to 30 ns. It was observed that the RMSDs of both systems reached to equilibrium and there was a progressive increase in RMSD until 3 ns with *Ld*MAP2 RMSD increasing to approximately 0.33 Å at approximately 3.5 ns. The *Ld*MAP2-bestatin complex marked a dip in RMSD at 8 ns and a sharp rise at 20 ns followed by a dip towards the end of MDS. As shown in the Fig. 9A, both *Ld*MAP2 and *Ld*MAP2-bestatin complex were stable throughout the 30 ns MDS run with the *Ld*MAP2-bestatin complex having contrastingly lesser fluctuation towards the end. The flexibility of the protein during MDS was investigated by calculating RMSF values of free *Ld*MAP2 and *Ld*MAP2-bestatin complex. The RMSF (in nm) was plotted against residue numbers on a 30 ns trajectory and clearly indicated that *Ld*MAP2-bestatin complex had lower fluctuations than native *Ld*MAP2. The non-catalytic residues (Y351, P354, T355 and E358) at C-terminus of the protein in *Ld*MAP2-bestatin complex showed greater fluctuations. Since the fluctuating residues do not make up the catalytic site and the catalytic residues in the complex have less fluctuation, it can be asserted that the structure of *Ld*MAP2 active site in the complex stood rigid during MDS (Fig. 9B).

The compactness of *Ld*MAP2 and *Ld*MAP2-bestatin complex was analyzed by plotting Rg values against time. The radius of gyration (Rg) which describes the overall mobility of the molecules and can be referred to as the root-mean-square distance of atomic assemblies from

their common centre of gravity was determined and plotted. A thorough analysis revealed that the Rg values to be stable for both native *Ld*MAP2 and *Ld*MAP2-bestatin complex throughout the 30 ns MDS run and pointed towards negligible fluctuations. This steadiness highlights that the stability, folding and compactness of the protein to be almost similar with and without bestatin (Fig. 9C). Therefore, the results depict that the MD simulations achieved equilibrium after 25 ns and emphasize that bestatin binds to *Ld*MAP2 in MD simulations due to a probable change in the microenvironment of *Ld*MAP2 which leads to conformational changes in the *Ld*MAP2 structure. This was reaffirmed by the changes in the secondary structure seen during MDS after analysis with the program DSSP [74] (Fig. 9D). All results obtained are substantiated by the results of circular dichroism where we noted changes in the secondary structural elements of *Ld*MAP2 upon binding of substrates and bestatin.

Therefore, from the MD simulation data we conclude that *Ld*MAP2-bestatin complex was stabilized by conformational rearrangements in the structure of *Ld*MAP2. It was also found that the binding of bestatin to *Ld*MAP2 slightly recasts the loop regions connecting the β-sheets and helices at the active site pocket. Bestatin interacts with *Ld*MAP2 majorly through hydrogen bonding and conformational adjustments in the protein structure. Thus, the results of CD are in close agreement with the MD simulations results as both suggest the occurrence of conformational changes in the *Ld*MAP2 upon bestatin binding. Such conformational changes have previously been reported for the *E. coli* aminopeptidase N upon bestatin binding [75].

Conclusions

In conclusion, we purified *Ld*MAP2 to homogeneity, analysed its metal dependence, enzymatic characteristics and substrate preferences. Our findings from biochemical assays asserted that *Ld*MAP2 functions optimally at physiological pH and its activity was enhanced

by divalent cations with cobalt emerging as the major enhancer for amidolytic activity. We then underscored the need to repurpose bestatin as a prodrug as it potently inhibited *Ld*MAP2. Additionally, CD studies revealed that bestatin and fluorogenic substrates increase the α-helical and β-sheet contents of *Ld*MAP2. Molecular docking suggested that the *Ld*MAP2-bestatin complex was stabilized by the hydrophobic interactions and hydrogen bonding. Furthermore, structural studies indicated that the catalytic pocket of *Ld*MAP2 is different from its human counterpart and suggested different binding modes of two orthologs with bestatin. This substantiates the idea that *Ld*MAP2 can be a potential druggable target to design and develop novel antileishmanials. Our studies provide important insights into the structure of *Ld*MAP2 and critical quantitative and mechanistic data on the binding affinity of bestatin with *Ld*MAP2 which may guide bestatin based drugs against leishmaniasis.

Author Contributions

This manuscript was drafted by SYB who also conducted experiments for this study with help of AD. IAQ conceived, designed and supervised the study. All authors critically reviewed the work and manuscript.

Acknowledgements

This work was supported by a grant awarded to Dr. Insaf A. Qureshi by the Council of Scientific and Industrial Research, India (CSIR, project no. 37(1686)/17/EMR-II), Government of India. The authors are grateful to the University of Hyderabad in general for Fellowship and Department of Biotechnology and Bioinformatics, University of Hyderabad in particular for extending facilities and support for this work. The authors are also thankful to Prof. Swati Saha for providing genomic DNA of *Leishmania donovani* as well as Drs. N.P. Prabhu, Mohd. Akif and M. Venkataramana for their suggestions during this work.

Conflict of interest

The authors hereby declare to have no conflict of interest whatsoever.

References

[1] B.L. Herwaldt, Leishmaniasis, Lancet. 354 (1999) 1191–1199. doi:10.1016/S0140-6736(98)10178-2.

[2] World Health Organization, Control of the leishmaniases: Report of a meeting of the WHO Expert Committee on the Control OF Leishmaniasis. GENEVA, World Health Organ. Tech. Rep. Ser. (2010) 185. doi:https://goo.gl/6iYa7H.

[3] J. Alvar, I.D. Vélez, C. Bern, M. Herrero, P. Desjeux, J. Cano, J. Jannin, M. de Boer, Leishmaniasis worldwide and global estimates of its incidence, PLoS One. 7 (2012). doi:10.1371/journal.pone.0035671.

[4] S. Sundar, Drug resistance in Indian visceral leishmaniasis, Trop. Med. Int. Heal. 6 (2001) 849–854. doi:10.1046/j.1365-3156.2001.00778.x.

[5] S. Mohapatra, Drug resistance in leishmaniasis: Newer developments, Trop. Parasitol. 4 (2014) 4. doi:10.4103/2229-5070.129142.

[6] a Taylor, Aminopeptidases: structure and function., FASEB J. 7 (1993) 290–298. doi:10.1186/1750-1326-5-48.

[7] T. Gonzales, J. Robert-Baudouy, Bacterial aminopeptidases: properties and functions, FEMS Microbiol. Rev. 18 (1996) 319–344. doi:10.1016/0168-6445(96)00020-4.

[8] M. Hildebrandt, G. International Conference on Dipeptidyl Aminopeptidases (2002 : Berlin, Dipeptidyl aminopeptidases in health and disease, 2003. doi:10.1007/b105297.

[9] P. Selvakumar, A. Lakshmikuttyamma, J.R. Dimmock, R.K. Sharma, Methionine aminopeptidase 2 and cancer, Biochim. Biophys. Acta - Rev. Cancer. 1765 (2006)

148–154. doi:10.1016/j.bbcan.2005.11.001.

[10] T.S. Skinner-Adams, J. Lowther, F. Teuscher, C.M. Stack, J. Grembecka, A. Mucha, P. Kafarski, K.R. Trenholme, J.P. Dalton, D.L. Gardiner, Identification of phosphinate dipeptide analog inhibitors directed against the *Plasmodium falciparum* M17 leucine aminopeptidase as lead antimalarial compounds, J. Med. Chem. 50 (2007) 6024–6031. doi:10.1021/jm070733v.

[11] W.T. Lowther, B.W. Matthews, Structure and function of the methionine aminopeptidases, Biochim. Biophys. Acta - Protein Struct. Mol. Enzymol. 1477 (2000) 157–167. doi:10.1016/S0167-4838(99)00271-X.

[12] J. a Boutin, Myristoylation., Cell. Signal. 9 (1997) 15–35. doi:10.1016/S0898-6568(96)00100-3.

[13] X. Chen, S. Xie, S. Bhat, N. Kumar, T.A. Shapiro, J.O. Liu, Fumagillin and fumarranol interact with *P. falciparum* methionine aminopeptidase 2 and inhibit malaria parasite growth *in vitro* and *in vivo*, Chem. Biol. 16 (2009) 193–202. doi:10.1016/j.chembiol.2009.01.006.

[14] C. Giglione, A. Boularot, T. Meinnel, Protein N-terminal methionine excision, Cell. Mol. Life Sci. 61 (2004). doi:10.1007/s00018-004-3466-8.

[15] P.H. Hirel, M.J. Schmitter, P. Dessen, G. Fayat, S. Blanquet, Extent of N-terminal methionine excision from *Escherichia coli* proteins is governed by the side-chain length of the penultimate amino acid., Proc. Natl. Acad. Sci. U. S. A. 86 (1989) 8247–51. doi:10.1073/pnas.86.21.8247.

[16] A. Addlagatta, X. Hu, J.O. Liu, B.W. Matthews, Structural basis for the functional differences between type I and type II human methionine aminopeptidases, Biochemistry. 44 (2005) 14741–14749. doi:10.1021/bi051691k.

[17] R.A. Bradshaw, W.W. Brickey, K.W. Walker, N-terminal processing: The methionine aminopeptidase and N(alpha)-acetyl transferase families, Trends Biochem. Sci. 23 (1998) 263–267. doi:10.1016/S0968-0004(98)01227-4.

[18] B. Datta, M.K. Ray, D. Chakrabarti, D.E. Wylie, N.K. Gupta, Glycosylation of eukaryotic peptide chain initiation factor 2 (eIF-2)-associated 67-kDa polypeptide (p67) and its possible role in the inhibition of eIF-2 kinase-catalyzed phosphorylation of the eIF-2 alpha-subunit, J. Biol. Chem. 264 (1989) 20620–20624.

[19] S. Calcagno, C.D. Klein, N-Terminal methionine processing by the zinc-activated *Plasmodium falciparum* methionine aminopeptidase 1b, Appl. Microbiol. Biotechnol. 100 (2016) 7091–7102. doi:10.1007/s00253-016-7470-3.

[20] M. Chatterjee, N. Chatterjee, R. Datta, B. Datta, N.K. Gupta, Expression and activity of p67 are induced during heat shock, Biochem Biophys Res Commun. 249 (1998) 113–117. doi:10.1006/bbrc.1998.9056.

[21] V.M. D'souza, B. Bennett, A.J. Copik, R.C. Holz, Divalent metal binding properties of the methionyl aminopeptidase from *Escherichia coli*, Biochemistry. 39 (2000) 3817–3826.

[22] G. Yang, R.B. Kirkpatrick, T. Ho, G.F. Zhang, P.H. Liang, K.O. Johanson, D.J. Casper, M.L. Doyle, J.P. Marino, S.K. Thompson, W. Chen, D.G. Tew, T.D. Meek, Steady-state kinetic characterization of substrates and metal-ion specificities of the full-length and N-terminally truncated recombinant human methionine aminopeptidases (Type 2), Biochemistry. 40 (2001) 10645–10654. doi:10.1021/bi010806r.

[23] L. Meng, S. Ruebush, V.M. D'souza, A.J. Copik, S. Tsunasawa, R.C. Holz, Overexpression and divalent metal binding properties of the methionyl aminopeptidase

from *Pyrococcus furiosus*, Biochemistry. 41 (2002) 7199–7208. doi:10.1021/bi020138p.

[24] A. Marschner, C.D. Klein, Metal promiscuity and metal-dependent substrate preferences of *Trypanosoma brucei* methionine aminopeptidase 1, Biochimie. 115 (2015) 35–43. doi:10.1016/j.biochi.2015.04.012.

[25] X. Li, Y.-H. Chang, Amino-terminal protein processing in *Saccharomyces cerevisiae* is an essential function that requires two distinct methionine aminopeptidases, Proc. Natl. Acad. Sci. U.S.A. 92 (1995) 12357–12361. doi:10.1073/pnas.92.26.12357.

[26] S.Y. Chang, E.C. McGary, S. Chang, Methionine aminopeptidase gene of *Escherichia coli* is essential for cell growth, J. Bacteriol. 171 (1989) 4071–2.

[27] R. Kumar, K. Tiwari, V.K. Dubey, Methionine aminopeptidase 2 is a key regulator of apoptotic like cell death in *Leishmania donovani*, Sci. Rep. 7 (2017) 95. doi:10.1038/s41598-017-00186-9.

[28] M. Altmeyer, E. Amtmann, C. Heyl, A. Marschner, A.J. Scheidig, C.D. Klein, Beta-aminoketones as prodrugs for selective irreversible inhibitors of type-1 methionine aminopeptidases, Bioorganic Med. Chem. Lett. 24 (2014) 5310–5314. doi:10.1016/j.bmcl.2014.09.047.

[29] J.J. Alvarado, A. Nemkal, J.M. Sauder, M. Russell, D.E. Akiyoshi, W. Shi, S.C. Almo, L.M. Weiss, Structure of a microsporidian methionine aminopeptidase type 2 complexed with fumagillin and TNP-470, Mol. Biochem. Parasitol. 168 (2009) 158–167. doi:10.1016/j.molbiopara.2009.07.008.

[30] E. Brakenhielm, Angiogenesis inhibitor, TNP-470, prevents diet-induced and genetic obesity in mice, Circ. Res. 94 (2004) 1579–1588. doi:10.1161/01.RES.0000132745.76882.70.

[31] Y.M. Kim, J.J. An, Y.J. Jin, Y. Rhee, B.S. Cha, H.C. Lee, S.K. Lim, Assessment of the anti-obesity effects of the TNP-470 analog CKD-732, J. Mol. Endocrinol. 38 (2007) 455–465. doi:10.1677/jme.1.02165.

[32] F. Frottin, W. V. Bienvenut, J. Bignon, E. Jacquet, A. Sebastian Vaca Jacome, A. Van Dorsselaer, S. Cianferani, C. Carapito, T. Meinnel, C. Giglione, MetAP1 and MetAP2 drive cell selectivity for a potent anti-cancer agent in synergy, by controlling glutathione redox state, Oncotarget. 7 (2016) 63306–63323. doi:10.18632/oncotarget.11216.

[33] J.W. Stern, J. Fang, S. Shusterman, G. Pierson, R. Barr, B. Pawel, L. Diller, S.A. Grupp, Angiogenesis inhibitor TNP-470 during bone marrow transplant: safety in a preclinical model, Clin. Cancer Res. 7 (2001) 1026–1032.

[34] C.S. Rutland, K. Jiang, G.A. Soff, C.A. Mitchell, Maternal administration of anti-angiogenic agents, TNP-470 and angiostatin4.5, induces fetal microphthalmia, Mol. Vis. 15 (2009) 1260–1269. doi:134 [pii].

[35] R. Satchi-Fainaro, M. Puder, J.W. Davies, H.T. Tran, D.A. Sampson, A.K. Greene, G. Corfas, J. Folkman, Targeting angiogenesis with a conjugate of HPMA copolymer and TNP-470, Nat. Med. 10 (2004) 255–261. doi:10.1038/nm1002.

[36] R.D. Finn, A. Bateman, J. Clements, P. Coggill, R.Y. Eberhardt, S.R. Eddy, A. Heger, K. Hetherington, L. Holm, J. Mistry, E.L.L. Sonnhammer, J. Tate, M. Punta, Pfam: the protein families database, Nucleic Acids Res. 42 (2014) D222-230. doi:10.1093/nar/gkt1223.

[37] K.D. Tsirigos, C. Peters, N. Shu, L. Käll, A. Elofsson. The TOPCONS web server for consensus prediction of membrane protein topology and signal peptides. Nucleic Acids Res. 43 (2015) W401-407. doi:10.1093/nar/gkv485.

[38] E. Gasteiger, C. Hoogland, A. Gattiker, S. Duvaud, M.R. Wilkins, R.D. Appel, A. Bairoch, Protein Identification and Analysis Tools on the ExPASy Server, in: J.M. Walker (Ed), The Proteomics Protocols Handbook, Humana Press 2005, pp. 571-607.

[39] J. González-Bacerio, J. Osuna, A. Ponce, R. Fando, K. Figarella, Y. Méndez, J.L. Charli, M.D.L.Á. Chávez, High-level expression in *Escherichia coli*, purification and kinetic characterization of *Plasmodium falciparum* M1-aminopeptidase, Protein Expr. Purif. 104 (2014) 103–114. doi:10.1016/j.pep.2014.08.002.

[40] J. Zheng, Z. Cheng, H. Jia, Y. Zheng, Characterization of aspartyl aminopeptidase from *Toxoplasma gondii*, Sci. Rep. 6 (2016) 34448. doi:10.1038/srep34448.

[41] L. Whitmore, B.A. Wallace, DICHROWEB, an online server for protein secondary structure analyses from circular dichroism spectroscopic data, Nucleic Acids Res. 32 (2004) W668-73. doi:10.1093/nar/gkh371.

[42] A. Sali, MODELLER A Program for Protein Structure Modeling Release 9v4, r6262, Structure. (2008) 779–815.

[43] A. Fiser, A. Sali, ModLoop: Automated modeling of loops in protein structures, Bioinformatics. 19 (2003) 2500–2501. doi:10.1093/bioinformatics/btg362.

[44] D. Van Der Spoel, E. Lindahl, B. Hess, G. Groenhof, A.E. Mark, H.J.C. Berendsen, GROMACS: Fast, flexible, and free, J. Comput. Chem. 26 (2005) 1701–1718. doi:10.1002/jcc.20291.

[45] W. Wang, M. Xia, J. Chen, F. Deng, R. Yuan, X. Zhang, F. Shen, Data set for phylogenetic tree and RAMPAGE Ramachandran plot analysis of SODs in *Gossypium raimondii* and *G. arboreum*, Data Br. 9 (2016) 345–348. doi:10.1016/j.dib.2016.05.025.

[46] W.L. DeLano, The PyMOL Molecular Graphics System, Schrödinger LLC

Wwwpymolorg. Version 1. (2002) http://www.pymol.org. doi:citeulike-article-id:240061.

[47] O. Trott, A.J. Olson, AutoDock Vina, J. Comput. Chem. 31 (2010) 445–461. doi:10.1002/jcc.21334.

[48] S. Kim, P.A. Thiessen, E.E. Bolton, J. Chen, G. Fu, A. Gindulyte, L. Han, J. He, S. He, B.A. Shoemaker, J. Wang, B. Yu, J. Zhang, S.H. Bryant, PubChem substance and compound databases, Nucleic Acids Res. 44 (2016) D1202–1213. doi:10.1093/nar/gkv951.

[49] San Diego: Accelrys Software Inc., Discovery Studio Modeling Environment, Release 3.5, Accelrys Softw. Inc. (2012).

[50] P. Alam, S.K. Chaturvedi, M.K. Siddiqi, R.K. Rajpoot, M.R. Ajmal, M. Zaman, R.H. Khan, Vitamin k3 inhibits protein aggregation: Implication in the treatment of amyloid diseases, Sci. Rep. 6 (2016) 26759. doi:10.1038/srep26759.

[51] M. Gokara, V. V. Narayana, V. Sadarangani, S.R. Chowdhury, S. Varkala, D.B. Ramachary, R. Subramanyam, Unravelling the binding mechanism and protein stability of human serum albumin while interacting with nefopam analogues: a biophysical and *in silico* approach, J. Biomol. Struct. Dyn. 35 (2017) 2280–2292. doi:10.1080/07391102.2016.1216895.

[52] D.M.F. van Aalten, R. Bywater, J.B.C. Findlay, M. Hendlich, R.W.W. Hooft, G. Vriend, PRODRG, a program for generating molecular topologies and unique molecular descriptors from coordinates of small molecules, J. Comput. Aided. Mol. Des. 10 (1996) 255–262. doi:10.1007/BF00355047.

[53] S. Liu, J. Widom, C.W. Kemp, C.M. Crews, J. Clardy, Structure of human methionine aminopeptidase-2 complexed with fumagillin., Science. 282 (1998) 1324–1327.

doi:10.1126/science.282.5392.1324.

[54] P. Zhang, D.E. Nicholson, J.M. Bujnicki, X. Su, J.J. Brendle, M. Ferdig, D.E. Kyle, W.K. Milhous, P.K. Chiang, Angiogenesis inhibitors specific for methionine aminopeptidase 2 as drugs for malaria and leishmaniasis, J. Biomed. Sci. 9 (2002) 34–40. doi:10.1159/000048197.

[55] Z.-Q. Ma, S.-X. Xie, Q.-Q. Huang, F.-J. Nan, T.D. Hurley, Q.-Z. Ye, Structural analysis of inhibition of *E. coli* methionine aminopeptidase: implication of loop adaptability in selective inhibition of bacterial enzymes, BMC Struct. Biol. 7 (2007) 84. doi:10.1186/1472-6807-7-84.

[56] J. Wang, K.A. Stieglitz, E.R. Kantrowitz, Metal specificity is correlated with two crucial active site residues in *Escherichia coli* alkaline phosphatase, Biochemistry. 44 (2005) 8378–8386. doi:10.1021/bi050155p.

[57] O. Kleifeld, L. Rulíšek, O. Bogin, A. Frenkel, Z. Havlas, Y. Burstein, I. Sagi, Higher metal-ligand coordination in the catalytic site of cobalt-substituted *Thermoanaerobacter brockii* alcohol dehydrogenase lowers the barrier for enzyme catalysis, Biochemistry. 43 (2004) 7151–7161. doi:10.1021/bi0302696.

[58] D.R. Holland, A.C. Hausrath, D. Juers, B.W. Matthews, Structural analysis of zinc substitutions in the active site of thermolysin, Protein Sci. 4 (1995) 1955–1965. doi:10.1002/pro.5560041001.

[59] H. Umezawa, T. Aoyagi, H. Suda, M. Hamada, T. Takeuchi, Bestatin, an inhibitor of aminopeptidase B, produced by actinomycetes., J. Antibiot. (Tokyo). 29 (1976) 97–99. doi:10.7164/antibiotics.29.97.

[60] R.E. Morty, J. Morehead, Cloning and characterization of a leucyl aminopeptidase from three pathogenic *Leishmania* species, J. Biol. Chem. 277 (2002) 26057–26065.

doi:10.1074/jbc.M202779200.

[61] K. Sekine, H. Fujii, F. Abe, Induction of apoptosis by bestatin (ubenimex) in human leukemic cell lines., Leukemia. 13 (1999) 729–34. doi:10.1038/sj.leu.2401388.

[62] Y. Hirayama, S. Sakamaki, N. Takayanagi, Y. Tsuji, T. Sagawa, H. Chiba, T. Matsunaga, Y. Niitsu, [Chemotherapy with ubenimex corresponding to patient age and organ disorder for 18 cases of acute myelogeneous leukemia in elderly patients--effects, complications and long-term survival], Gan To Kagaku Ryoho. 30 (2003) 1113–1118.

[63] Y. Aozuka, K. Koizumi, Y. Saitoh, Y. Ueda, H. Sakurai, I. Saiki, Anti-tumor angiogenesis effect of aminopeptidase inhibitor bestatin against B16-BL6 melanoma cells orthotopically implanted into syngeneic mice, Cancer Lett. 216 (2004) 35–42. doi:10.1016/j.canlet.2004.06.050.

[64] F. Abe, G. Alvord, M. Koyama, A. Matsuda, J.E. Talmadge, Pharmacokinetics of bestatin and oral activity for treatment of experimental metastases, Cancer Immunol. Immunother. 28 (1989) 29–33. doi:10.1007/BF00205797.

[65] S. Labbe, D. Grenier, P. Plamondon, V.J. Uitto, D. Mayrand, Effects of dipeptide bestatin on *Porphyromonas gingivalis* and epithelial cells, J Periodontol. 72 (2001) 714–721. doi:10.1902/jop.2001.72.6.714.

[66] G. Pulido-Cejudo, B. Conway, P. Proulx, R. Brown, C.A. Izaguirre, Bestatin-mediated inhibition of leucine aminopeptidase may hinder HIV infection, Antiviral Res. 36 (1997) 167–177. doi:10.1016/S0166-3542(97)00052-1.

[67] S.K. Burley, P.R. David, W.N. Lipscomb, Leucine aminopeptidase: bestatin inhibition and a model for enzyme-catalyzed peptide hydrolysis., Proc. Natl. Acad. Sci. U.S.A. 88 (1991) 6916–6920. doi:10.1073/pnas.88.16.6916.

[68] J.-Y. Lee, S.-M. Song, J.-W. Seok, B.K. Jha, E.-T. Han, H.-O. Song, H.-S. Yu, Y. Hong, H.-H. Kong, D.-I. Chung, M17 leucine aminopeptidase of the human malaria parasite *Plasmodium vivax*, Mol. Biochem. Parasitol. 170 (2010) 45–48. doi:10.1016/j.molbiopara.2009.11.003.

[69] A.A. Nickson, K.E. Stoll, J. Clarke, Folding of a LysM domain: entropy-enthalpy compensation in the transition state of an ideal two-state folder, J. Mol. Biol. 380 (2008) 557–569. doi:10.1016/j.jmb.2008.05.020.

[70] J.M. Prescott, F.W. Wagner, B. Holmquist, B.L. Vallee, Spectral and kinetic studies of metal-substituted aeromonas aminopeptidase: nonidentical, interacting metal-binding sites, Biochemistry. 24 (1985) 5350–5356. doi:10.1021/bi00341a012.

[71] P. Alam, A.S. Abdelhameed, R.K. Rajpoot, R.H. Khan, Interplay of multiple interaction forces: Binding of tyrosine kinase inhibitor nintedanib with human serum albumin, J. Photochem. Photobiol. B Biol. 157 (2016) 70–76. doi:10.1016/j.jphotobiol.2016.02.009.

[72] J. Timm, M. Valente, D. García-Caballero, K.S. Wilson, D. González-Pacanowska, Structural characterization of acidic M17 leucine aminopeptidases from the TriTryps and evaluation of their role in nutrient starvation in *Trypanosoma brucei*, mSphere. 2 (2017) e00226-17. doi:10.1128/mSphere.00226-17.

[73] M.B. Harbut, G. Velmourougane, S. Dalal, G. Reiss, J.C. Whisstock, O. Onder, D. Brisson, S. McGowan, M. Klemba, D.C. Greenbaum, Bestatin-based chemical biology strategy reveals distinct roles for malaria M1- and M17-family aminopeptidases., Proc. Natl. Acad. Sci. U.S.A. 108 (2011) E526–E534. doi:10.1073/pnas.1105601108.

[74] J. Zacharias, E.W. Knapp, Protein secondary structure classification revisited: Processing DSSP information with PSSC, J. Chem. Inf. Model. 54 (2014) 2166–2179.

doi:10.1021/ci5000856.

[75] K. Ito, Y. Nakajima, Y. Onohara, M. Takeo, K. Nakashima, F. Matsubara, T. Ito, T. Yoshimoto, Crystal structure of aminopeptidase N (Proteobacteria alanyl aminopeptidase) from *Escherichia coli* and conformational change of methionine 260 involved in substrate recognition, J. Biol. Chem. 281 (2006) 33664–33676. doi:10.1074/jbc.M605203200.

Table 1) Steady state kinetic parameters of *Ld*MAP2 with six divalent cations at 37°C: The parameters were obtained from a 60 minutes kinetic cycle performed in triplicates for each divalent metal cation. The data suggested *Ld*MAP2 to be a Co(II) activated protein. However, the *Ld*MAP2 activity was also driven by physiologically abundant metals like Mg^{2+}, Mn^{2+} and Ca^{2+}.

Metal ion	**Concentration (µM)**	**K_m (µM)**	**k_{cat} (min^{-1})**	**k_{cat}/K_m ($\mu M^{-1} min^{-1}$)**
Co^{2+}	100	154.1±12.35	128.1±4	0.83
Mg^{2+}	100	179.2±14.47	109.2±6.9	0.60
Mn^{2+}	100	166.9±14.35	99.9±4.8	0.59
Ca^{2+}	100	124.7±9.21	89.89±3.8	0.72
Ni^{2+}	100	284.4±33.13	88.4±8.9	0.31
Cu^{2+}	100	171.9±17.56	26±3.5	0.15

Legends:

Figure 1) Sequence alignment of *Ld*MAP2 with *Hs*MAP2: The sequence alignment of *Ld*MAP2 with *Hs*MAP2 reveals a conserved active site between two orthologs (highlighted by blue stars). Notice the key differences in the two sequences particularly in the prosite motif (highlighted by a black line) as result of which two proteins attain different conformations and bind differently to inhibitor bestatin and aminopeptidase substrates.

Figure 2) Purification of *Ld*MAP2: Figure 2A shows the purification of *Ld*MAP2 followed by the cleavage of N-terminal SUMO tag by its overnight digestion with SUMO protease at 4°C. The undigested *Ld*MAP2-SUMO tag can be seen in lane 2 while lane 1 represents unstained protein standard. Lanes 3 and 4 displays *Ld*MAP2 before and after affinity chromatography on Ni-NTA agarose. Figure 2B depicts the gel permeation chromatogram of *Ld*MAP2 which suggested it to be a monomer.

Figure 3) Enzyme activity of purified *Ld*MAP2: Figure 3A shows the increase in florescence with time in a kinetic cycle that lasted 60 minutes at 37°C with Co(II) as cofactor in the assay buffer. Figure 3B shows enzyme assay of *Ld*MAP2in which the fluorogenic substrate Ala-AMC was used to a final concentration of 400 μM. Figure 3C depicts the enzyme kinetic assays carried out with 6 metal chlorides. One activity unit was defined as AMC (pM) released per mg of recombinant *Ld*MAP2 protein.

Figure 4) Metal dependence, pH profile, temperature stability and substrate preference of *Ld*MAP2: Figure 4A and 4B represents the metal ion dependence of *Ld*MAP2 in the concentration range of 0 to 10 mM. The figure indicates that the recombinant *Ld*MAP2 had highest activity at lesser concentrations of divalent metal and that high concentrations were

inhibitory. Figures 4C and 4D show the pH optima of *Ld*MAP2 to be 7.5 while, figure 4E indicates that the optimum temperature for *Ld*MAP2 activity is between 30-40°C beyond which there is a sharp fall in activity. Figures 4F and 4H are the spectra taken at different temperatures in the range of 20 to 100°C for native and Ca(II) activated *Ld*MAP2. The ellipticity monitored at 208 nm suggested the native *Ld*MAP2 to be more heat stable than the metal activated one. Figure 4G indicates that the *Ld*MAP2 had better catalytic efficiency against the cleavage of smaller amino acid residue alanine from the synthetic substrates. The data is presented as mean ± SD of three experiments.

Figure 5) *Ld*MAP2 inhibition with the aminopeptidase inhibitor bestatin: Figure 5A shows the inhibition of *Ld*MAP2 with bestatin in the concentration range of 0 to 50 μM. Bestatin inhibited *Ld*MAP2 competitively which is evident from the Lineweaver-Burk plot. The competitive binding mode of bestatin was also confirmed by molecular docking studies. The parameters determined in figure 5A were used to calculate inhibitory constant (K_i) as shown in figure 5B. The data is presented as mean ± SD of three experiments.

Figure 6) CD spectroscopy: Figure 6A depicts the loss of ellipticity in the spectra taken upon the addition of urea. Notice complete denaturation of *Ld*MAP2 after 6M urea was added. Figure 6B shows a plot between fraction unfolded and Urea concentration which signified *Ld*MAP2 to be following two state model of folding with a Gibbs free energy (ΔG) of~ 2.2 kcal mol^{-1}. Figure 6C and 6D highlights the changes in the secondary structure of *Ld*MAP2 with the addition of bestatin and most preferred *Ld*MAP2 substrate (Ala-AMC), respectively. Both bestatin and Ala-AMC seemed to bind well to the LdMAP2 structure and thence contributed to the secondary structure. The changes were monitored at 208 and 222 nm and with the web-based software DICHROWEB. A similar result was obtained for other substrates.

Figure 7) Structure of *Ld*MAP2 and overlay of *Ld*MAP2 and *Hs*MAP2: Figure 7A shows the three dimensional structure of *Ld*MAP2. Figure 7B reflects the changes in conformation of *Ld*MAP2 caused by amino acid substitutions in the MAP2 prosite. These substitutions appear to make *Ld*MAP2 structurally different from *Hs*MAP2. However, the two structures have a conserved active site composed of residues DDHEE.

Figure 8) Interactions of bestatin with *Hs*MAP2 and *Ld*MAP2 and the binding interactions of substrates Ala-AMC, Leu-AMC and Met-AMC at the active site of *Ld*MAP2: Figures 8A and 8B depict the interactions of aminopeptidase inhibitor bestatin at the catalytic pocket of *Hs*MAP2 and *Ld*MAP2, respectively. The inhibitor bestatin seemed to have stronger interactions with *Ld*MAP2 as against *Hs*MAP2. Figure 8C shows the interaction of Ala-AMC with *Ld*MAP2. Figure 8D shows the interaction between Leu-AMC and *Ld*MAP2, while figure 8E depicts the binding of Met-AMC to *Ld*MAP2 at the catalytic site. Notice the difference in the binding pattern and the involvement of different residues in binding in each case. Notably, S217 and E252 was the common interacting residue for Leu-AMC and Met-AMC. Amongst three substrates, Ala-AMC had strongest interactions with *Ld*MAP2. The latter also showed highest catalytic efficiency against Ala-AMC.

Figure 9) Molecular dynamic studies of native *Ld*MAP2 and *Ld*MAP2-bestatin complex: Figures 9A and 9B show the RMSD and RMS fluctuations of native *Ld*MAP2 and *Ld*MAP-bestatin complex during 30 ns MDS. Figure 9C shows the residues mobility (Rg) of the two systems which recorded a similar stability and compactness pattern throughout the 30 ns MDS run. Figure 9D highlights the changes in the secondary structural elements of native *Ld*MAP2 and *Ld*MAP2-bestatin complex during molecular dynamics studies.

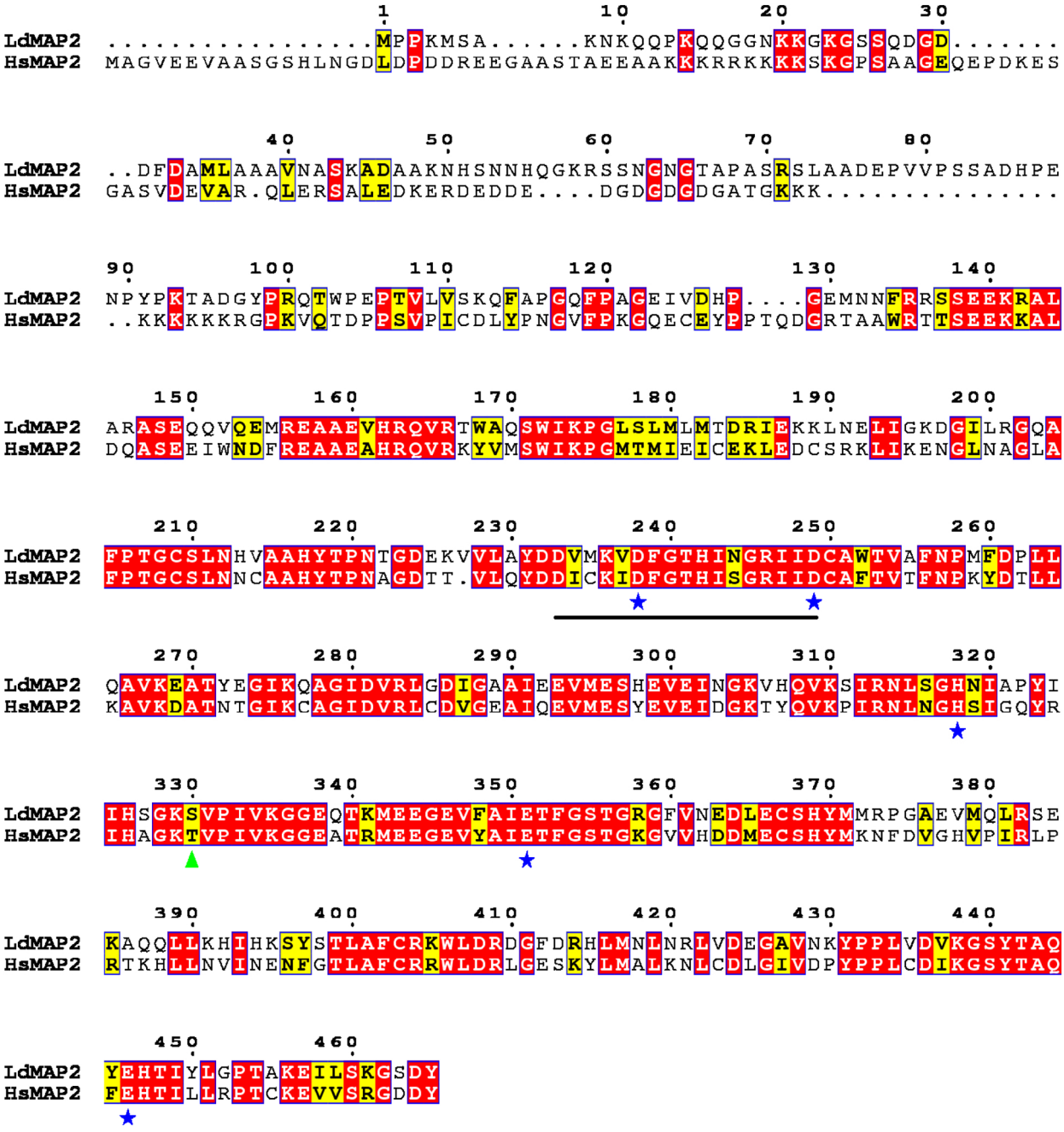
LdMAP2 ..... MPPKMSA..... KNKQQPKQQGGNKKGKGSSQDGD.....
HsMAP2 MAGVEEVAASGSHLNGDLDPDDREEGAASTAEEAAKKKRRKKKSKGPSAAGEQEPDKES
LdMAP2 ..DFDAMLAAAVNASKADAAKNHSNNHQGKRSSNGNGTAPASRSLAADEPVVPSSADHPE
HsMAP2 GASVDEVAR.QLERSALEDKERDEDDE....DGDGDGDGATGKKK.............
LdMAP2 NPYPKTADGYPRQTWPEPTVLVSKQFAPGQFPAGEIVDHP....GEMNNFRRSSEEKRAL
HsMAP2 ..KKKKKKRGPKVQTDPPSVPICDLYPNGVFPKGQECEYPPTQDGRTAAWRTTSEEKKAL
LdMAP2 ARASEQQVQEMREAAEVHRQVRTWAQSWIKPGLSLMLMTDRIEKKLNELIGKDGILRGQA
HsMAP2 DQASEEIWNDFREAAEAHRQVRKYVMSWIKPGMTMIEICEKLEDCSRKLIKENGLNAGLA
LdMAP2 FPTGCSLNHVAAHYTPNTGDEKVVLAYDDVMKVDFGTHINGRIIDCAWTVAFNPMFDPLL
HsMAP2 FPTGCSLNNCAAHYTPNAGDTT.VLQYDDICKIDFGTHISGRIIDCAFTVTFNPKYDTLL
LdMAP2 QAVKEATYEGIKQAGIDVRLGDIGAAIEEVMESHEVEINGKVHQVKSIRNLSGHNIAPYI
HsMAP2 KAVKDATNTGIKCAGIDVRLCDVGEAIQEVMESYEVEIDGKTYQVKPIRNLNGHSIGQYR
LdMAP2 IHSGKSVPIVKGGEQTKMEEGEVFAIETFGSTGRGFVNEDLECSHYMMRPGAEVMQLRSE
HsMAP2 IHAGKTVPIVKGGEATRMEEGEVYAIETFGSTGKGVVHDDMECSHYMKNFDVGHVPIRLP
LdMAP2 KAQQLLKHIHKSYSTLAFCRKWLDRDGFDRHLMNLNRLVDEGAVNKYPPLVDVKGSYTAQ
HsMAP2 RTKHLLNVINENFGTLAFCRRWLDRLGESKYLMALKNLCDLGIVDPYPPLCDIKGSYTAQ
LdMAP2 YEHTIYLGPTAKEILSKGSDY
HsMAP2 FEHTILLRPTCKEVVSRGDDY

Figure 1

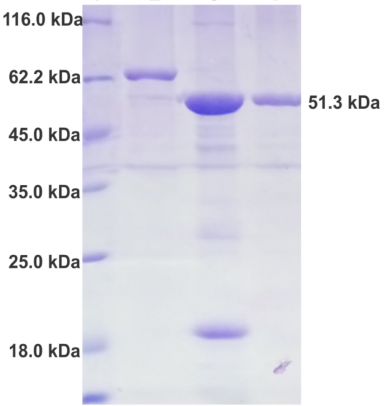
1
2
3
4
116.0 kDa
62.2 kDa
45.0 kDa
35.0 kDa
25.0 kDa
18.0 kDa
51.3 kDa

A

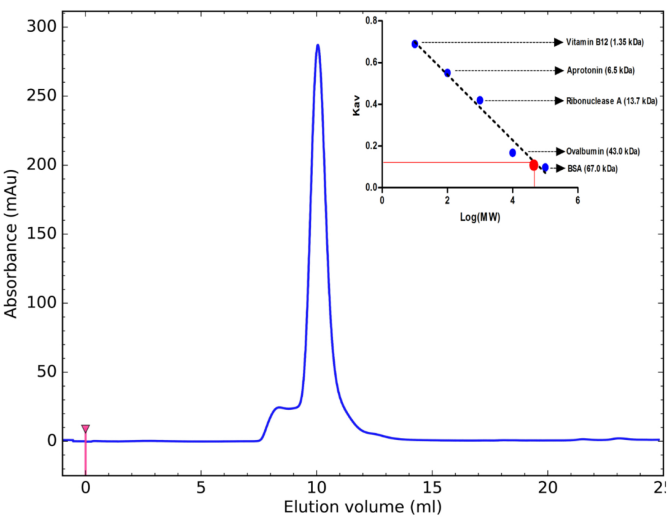
Absorbance (mAu)
Elution volume (ml)
Kav
Log(MW)
Vitamin B12 (1.35 kDa)
Aprotonin (6.5 kDa)
Ribonuclease A (13.7 kDa)
Ovalbumin (43.0 kDa)
BSA (67.0 kDa)

B

Figure 2

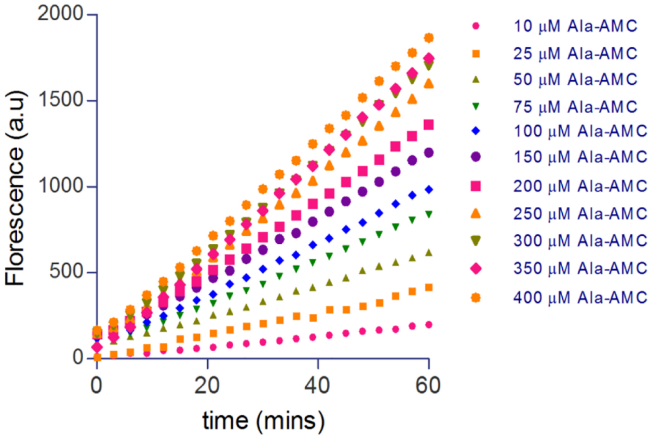
Florescence (a.u)
time (mins)
10 μM Ala-AMC
25 μM Ala-AMC
50 μM Ala-AMC
75 μM Ala-AMC
100 μM Ala-AMC
150 μM Ala-AMC
200 μM Ala-AMC
250 μM Ala-AMC
300 μM Ala-AMC
350 μM Ala-AMC
400 μM Ala-AMC

A

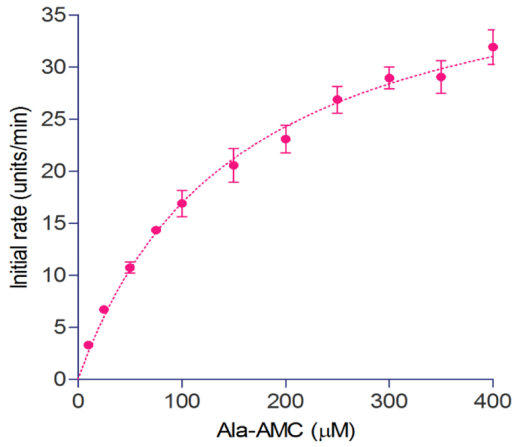
Initial rate (units/min)
Ala-AMC (μM)

B

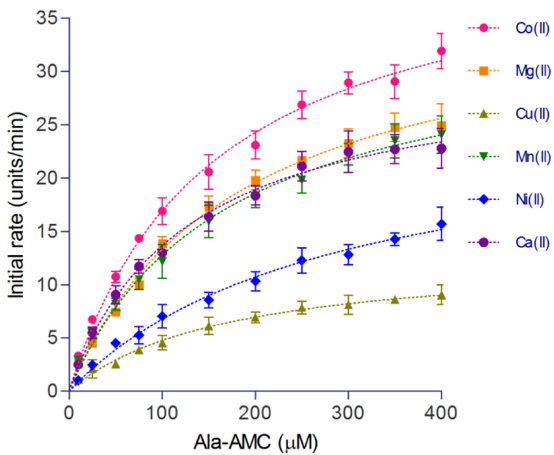
Initial rate (units/min)
Ala-AMC (μM)
Co(II)
Mg(II)
Cu(II)
Mn(II)
Ni(II)
Ca(II)

C

Figure 3

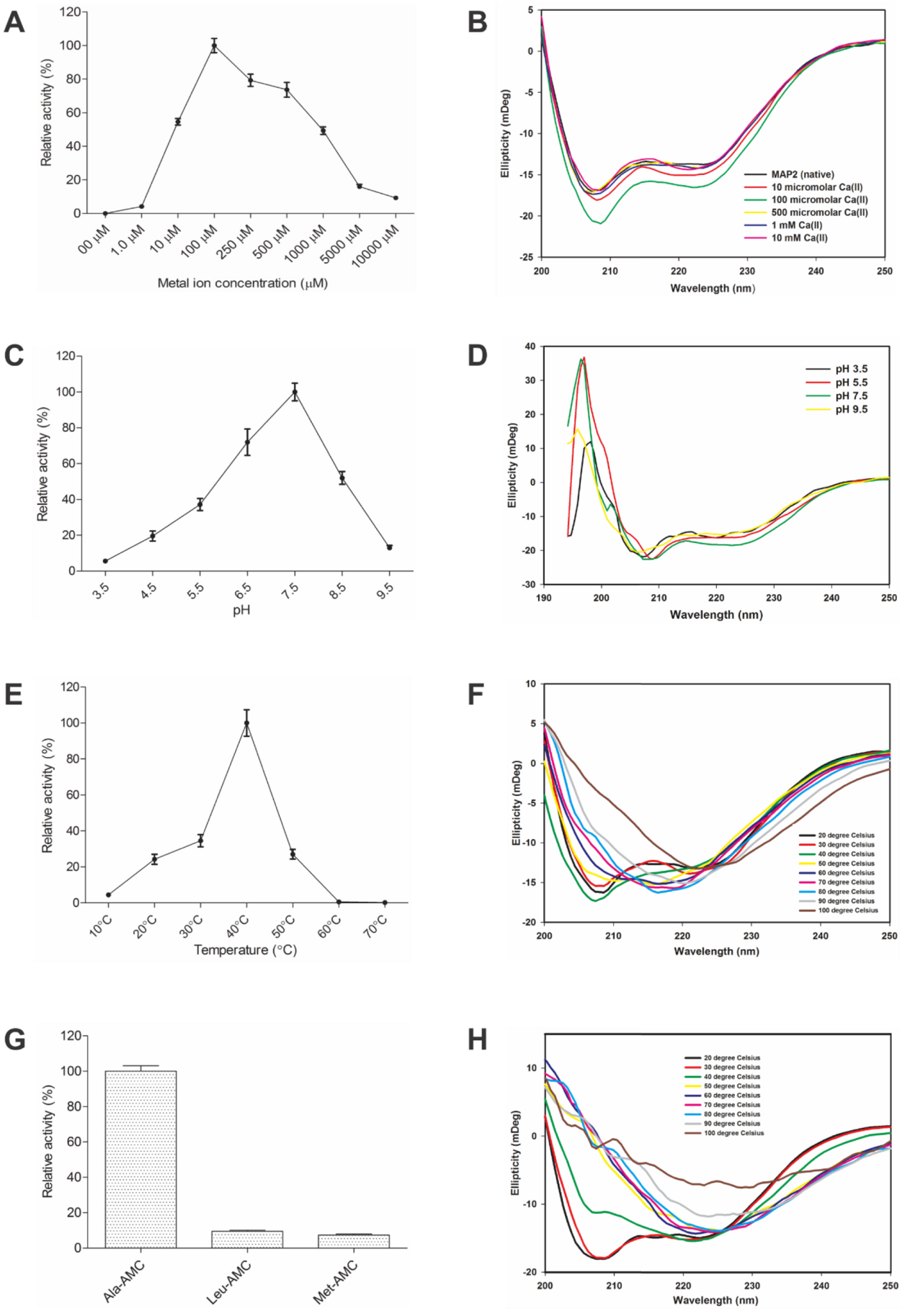
A
Relative activity (%)
120
100
80
60
40
20
0
00 µM
1.0 µM
10 µM
100 µM
250 µM
500 µM
1000 µM
5000 µM
10000 µM
Metal ion concentration (µM)
B
Ellipticity (mDeg)
5
0
-5
-10
-15
-20
-25
200
210
220
230
240
250
Wavelength (nm)
MAP2 (native)
10 micromolar Ca(II)
100 micromolar Ca(II)
500 micromolar Ca(II)
1 mM Ca(II)
10 mM Ca(II)
C
Relative activity (%)
120
100
80
60
40
20
0
3.5
4.5
5.5
6.5
7.5
8.5
9.5
pH
D
Ellipticity (mDeg)
40
30
20
10
0
-10
-20
-30
190
200
210
220
230
240
250
Wavelength (nm)
pH 3.5
pH 5.5
pH 7.5
pH 9.5
E
Relative activity (%)
120
100
80
60
40
20
0
10°C
20°C
30°C
40°C
50°C
60°C
70°C
Temperature (°C)
F
Ellipticity (mDeg)
10
5
0
-5
-10
-15
-20
200
210
220
230
240
250
Wavelength (nm)
20 degree Celsius
30 degree Celsius
40 degree Celsius
50 degree Celsius
60 degree Celsius
70 degree Celsius
80 degree Celsius
90 degree Celsius
100 degree Celsius
G
Relative activity (%)
120
100
80
60
40
20
0
Ala-AMC
Leu-AMC
Met-AMC
H
Ellipticity (mDeg)
10
0
-10
-20
200
210
220
230
240
250
Wavelength (nm)
20 degree Celsius
30 degree Celsius
40 degree Celsius
50 degree Celsius
60 degree Celsius
70 degree Celsius
80 degree Celsius
90 degree Celsius
100 degree Celsius

Figure 4

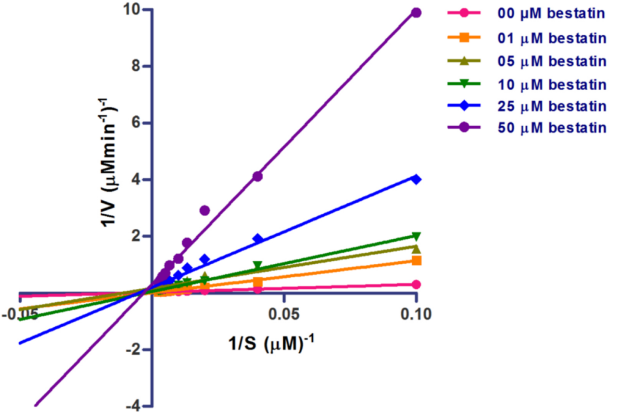
00 μM bestatin
01 μM bestatin
05 μM bestatin
10 μM bestatin
25 μM bestatin
50 μM bestatin
1/V (μMmin-1)-1
1/S (μM)-1
10
8
6
4
2
-2
-4
0.05
0.10

A

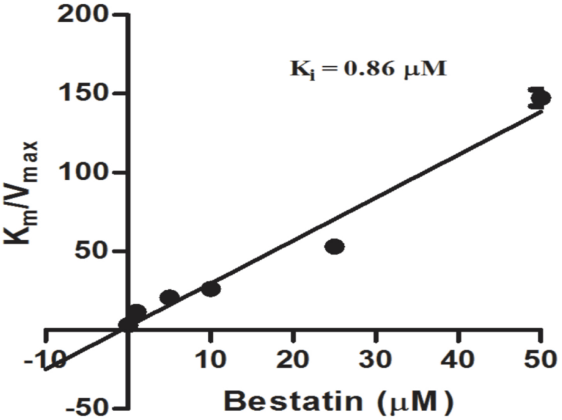
Ki = 0.86 μM
Km/Vmax
Bestatin (μM)
200
150
100
50
-50
-10
10
20
30
40
50

B

Figure 5

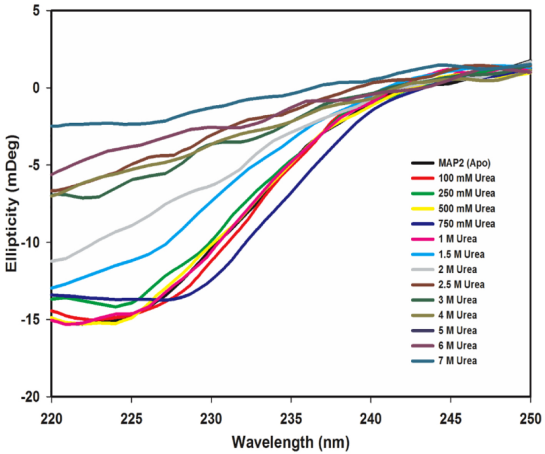

A

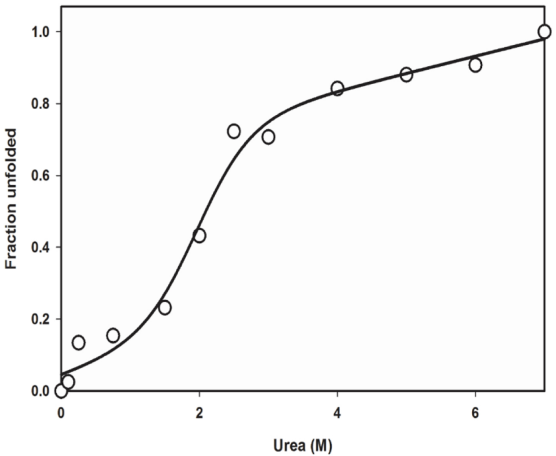

B

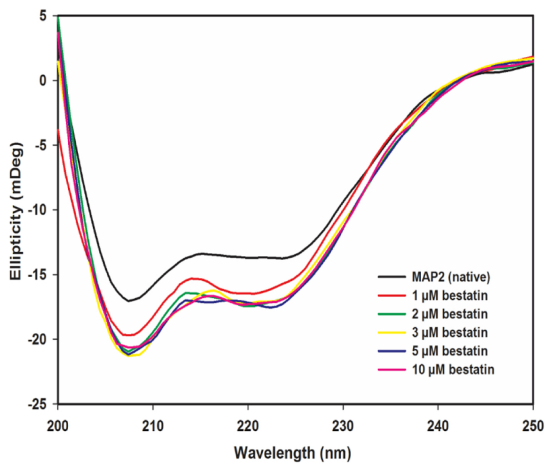

C

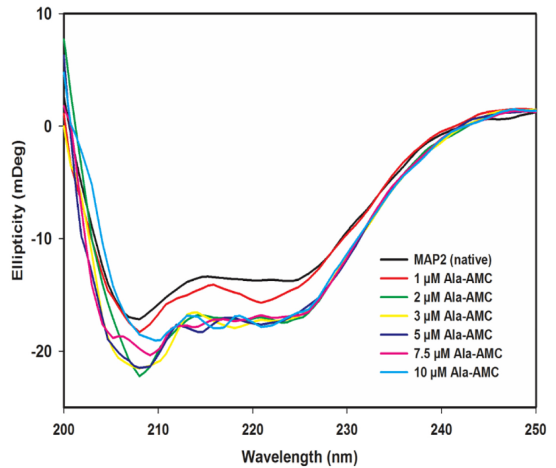

D

Figure 6

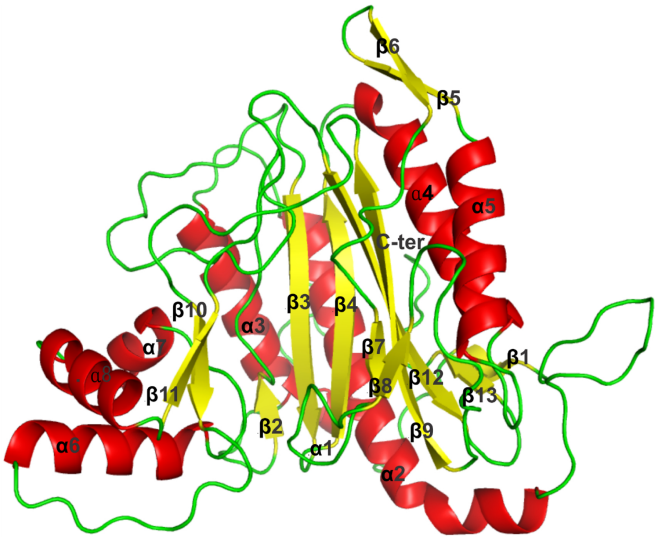
β6
β5
α4
α5
C-ter
β10
α3
β3
β4
α
β7
β1
α
β11
β8
β12
β13
β2
α1
β9
α6
α2

A

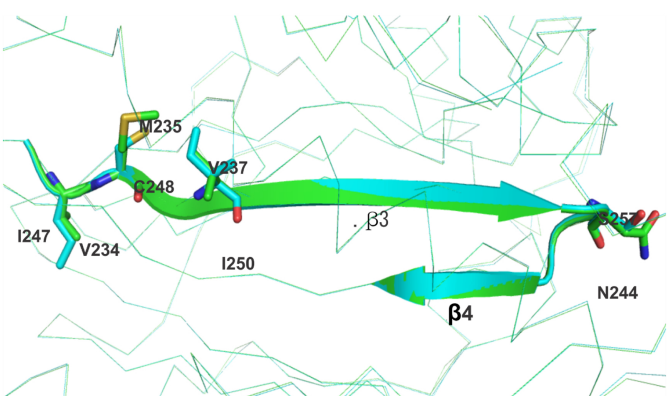
M235
V237
C248
I247
V234
I250
β3
N244
β4

B

Figure 7

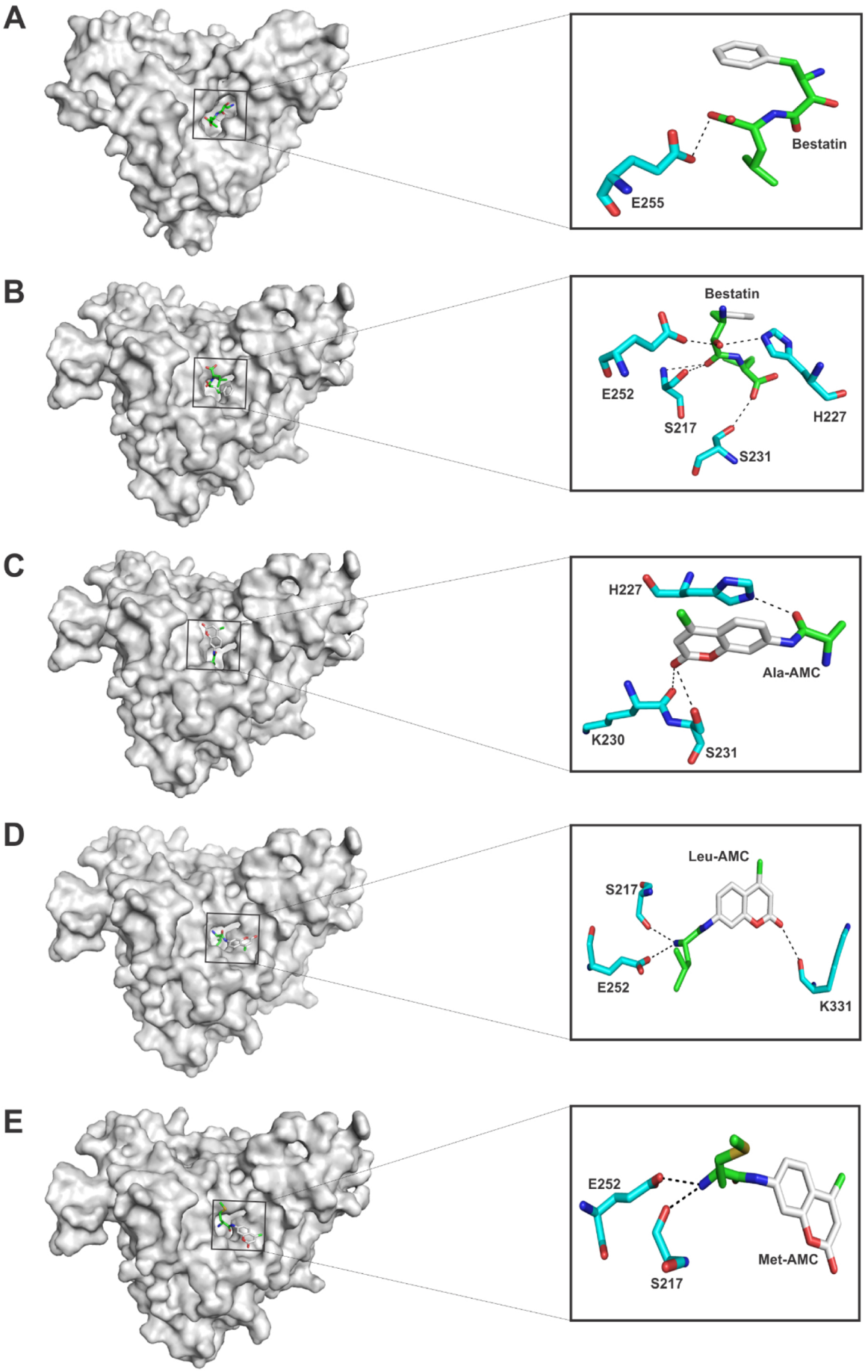
A
Bestatin
E255
B
Bestatin
E252
S217
H227
S231
C
H227
Ala-AMC
K230
S231
D
Leu-AMC
S217
E252
K331
E
E252
Met-AMC
S217

Figure 8

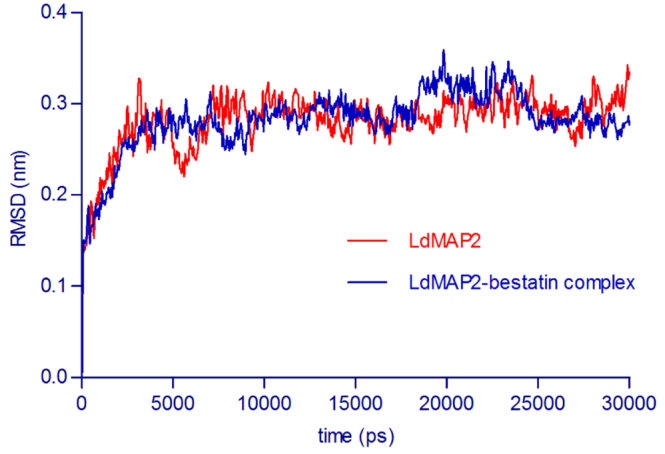

A

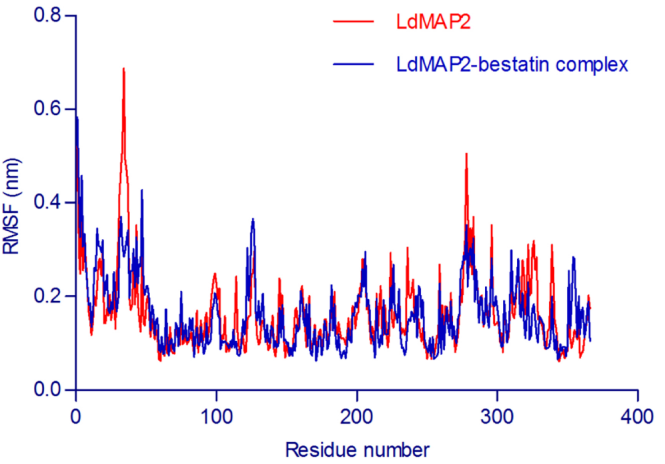

B

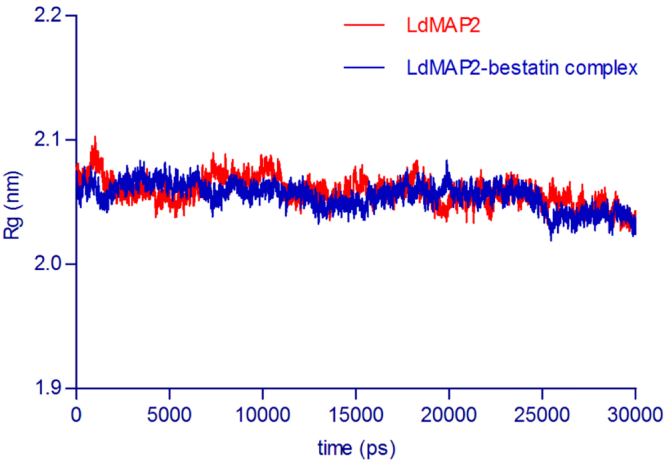

C

Figure 9ac

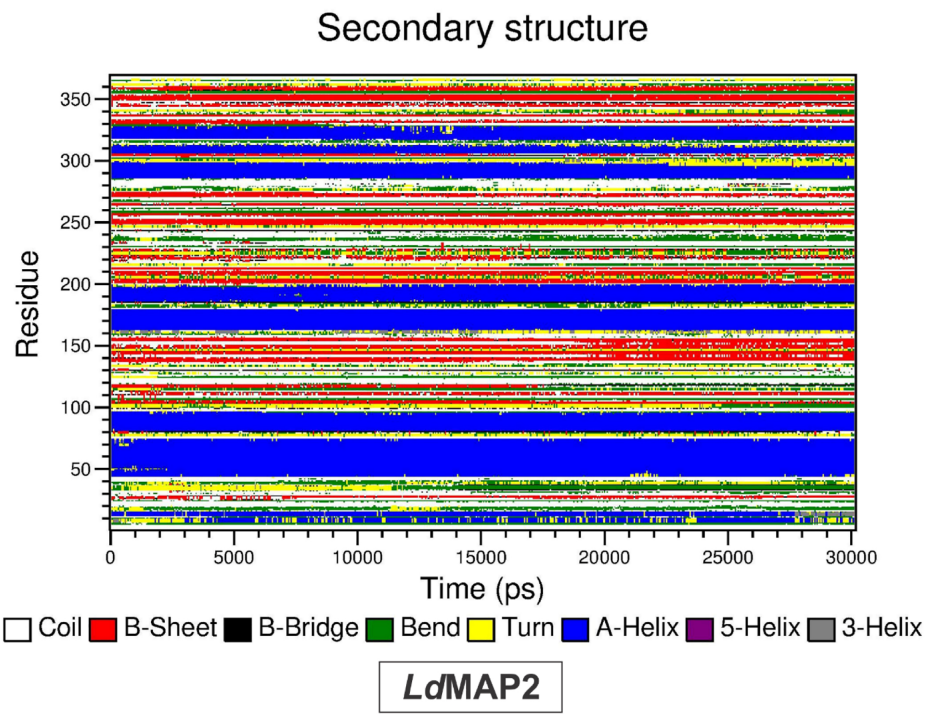
Secondary structure
Residue
350
300
250
200
150
100
50
0
5000
10000
15000
20000
25000
30000
Time (ps)
Coil
B-Sheet
B-Bridge
Bend
Turn
A-Helix
5-Helix
3-Helix
LdMAP2

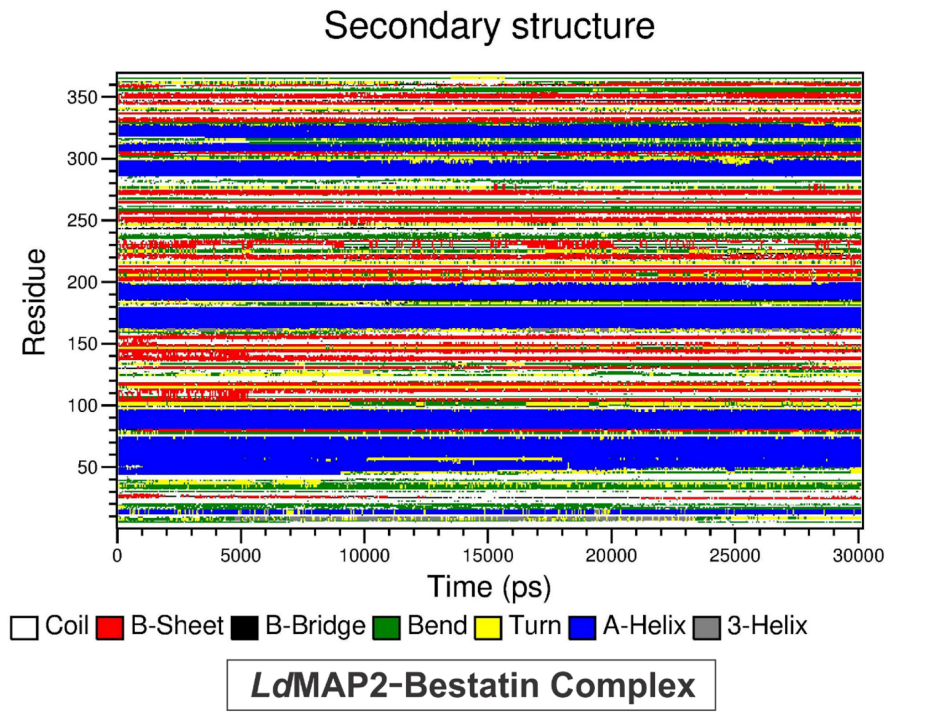
Secondary structure
Residue
350
300
250
200
150
100
50
0
5000
10000
15000
20000
25000
30000
Time (ps)
Coil
B-Sheet
B-Bridge
Bend
Turn
A-Helix
3-Helix
LdMAP2-Bestatin Complex

D

Figure 9d